Chinese Chemical Letters 37 (2026) 111937

Contents lists available at ScienceDirect

Chinese Chemical Letters

journal homepage: www.elsevier.com/locate/cclet

Folic acid-modified erythrocyte membrane enhances targeted delivery of biomimetic nanoplatforms for hepatocellular carcinoma therapy

Hang Xiao[1], Hongyu Zhong[1], Shiqi Yang[1], Kunwei Li, Jing Su, Faisal Raza*, Mingfeng Qiu*

School of Pharmaceutical Science, Shanghai Jiao Tong University, Shanghai 200240, China

ARTICLE INFO

Article history:
Received 21 July 2025
Revised 30 September 2025
Accepted 8 October 2025
Available online 10 October 2025

Keywords:
Liver cancer
Norcantharidin
Polyethylenimine
Erythrocyte membrane
Folic acid

ABSTRACT

Liver cancer, particularly hepatocellular carcinoma (HCC), is a leading cause of cancer-related mortality worldwide. The therapeutic potential of norcantharidin (NCTD), a small-molecule chemotherapeutic agent, is often limited by its rapid systemic clearance and dose-dependent nephrotoxicity. Here, a novel folic acid (FA)-modified erythrocyte membrane (EM)-coated nanoplatform (FA/EM@PEI-NCTD) was developed to improve tumor targeting, prolong circulation, and mitigate renal toxicity. This nanoplatform preserves CD47 expression, transmitting "don't eat me" signal to evade macrophage uptake. *In vitro*, FA/EM@PEI-NCTD showed enhanced cytotoxicity against HCC cells and favorable drug release kinetics with low hemolytic activity. *In vivo*, the system demonstrated superior tumor targeting, growth inhibition, prolonged survival, and reduced nephrotoxicity. Mechanistically, the treatment promoted apoptosis in H22 cells by upregulating Bax and caspase-3 while downregulating Bcl-2. These results highlight FA/EM@PEI-NCTD as a promising strategy for safe and effective targeted HCC therapy.

© 2026 Published by Elsevier B.V. on behalf of Chinese Chemical Society and Institute of Materia Medica, Chinese Academy of Medical Sciences.

Liver cancer ranks as the sixth most diagnosed cancer and the third leading cause of cancer-related mortality worldwide [1]. Among its subtypes, hepatocellular carcinoma (HCC) accounts for 75 %–85 % of cases and remains a major global health challenge [2–4]. Norcantharidin (NCTD), a small-molecule chemotherapeutic agent for HCC, has demonstrated the ability to induce apoptosis in tumor cells and elevate white blood cell counts [5–8]. However, its clinical application is limited by rapid systemic clearance and dose-dependent nephrotoxicity [6,9,10]. To overcome these limits, we combined nanotechnology and biomimetic strategies to develop a targeted and sustained-release delivery system for NCTD.

Initially, polyethyleneimine (PEI) was employed to synthesize NCTD-loaded nanoparticles (PEI-NCTD) due to its exceptionally high charge density, strong adsorption capacity, and high chemical reactivity, making it a highly promising material for drug delivery applications [11–13]. The infrared spectrum (Fig. 1a) confirmed the formation of amide bonds between PEI and NCTD, as evidenced by the disappearance of characteristic absorption peaks corresponding to acid anhydride carbonyl and primary amine groups, and the appearance of new amide peaks. As shown in Figs. 1b and e, PEI-NCTD demonstrated a uniform spherical morphology with a diameter of 88.66 ± 2.34 nm.

CD47 protein is abundantly expressed on erythrocyte membrane (EM) and can interact with signal regulatory protein α to transmit a "don't eat me" signal to the reticuloendothelial system (RES) [14,15]. Therefore, the systemic circulation of EM-coated nanoparticles could be prolonged [16–18]. We collected blood from male BALB/c mice and extracted *via* hypotonic lysis [17,19,20]. Subsequently, PEI-NCTD and EM were co-extruded through polycarbonate membrane to get EM-camouflage nanoparticles (EM@PEI-NCTD) [21]. As folic acid (FA) is overexpressed on the surface of liver cancer cells [22,23], we functionalized the surface of EM@PEI-NCTD with FA to further enhance tumor-targeting capability, obtaining the final drug delivery system (FA/EM@PEI-NCTD).

To confirm the successful encapsulation of PEI-NCTD within EM, we prepared empty membrane vesicles (EMVs) by extruding EM alone. From Fig. 1b, the average particle sizes of EMV and FA/EM@PEI-NCTD were 97.01 ± 3.83 and 99.90 ± 1.36 nm, respectively. The presence of a distinct membrane bilayer structure with a thickness of approximately 13 nm was clearly observed (Fig. 1g), consistent with previous report [20]. The polydispersity indices (PDIs) of PEI-NCTD, EMV, and FA/EM@PEI-NCTD were all below 0.3 (Fig. 1c), indicating favorable dispersion stability.

The EMV structure can be clearly seen in the TEM of Fig. 1f. In addition, zeta potential measurements confirmed the successful membrane encapsulation. PEI-NCTD exhibited a positive surface charge of 17.38 ± 1.26 mV, whereas EMV and FA/EM@PEI-NCTD showed negative charges of -26.69 ± 3.47 and -20.56 ± 5.21 mV,

* Corresponding authors.
E-mail addresses: faisalraza@sjtu.edu.cn (F. Raza), mfqiu@sjtu.edu.cn (M. Qiu).
[1] These authors contributed equally to this work.

https://doi.org/10.1016/j.cclet.2025.111937
1001-8417/© 2026 Published by Elsevier B.V. on behalf of Chinese Chemical Society and Institute of Materia Medica, Chinese Academy of Medical Sciences.

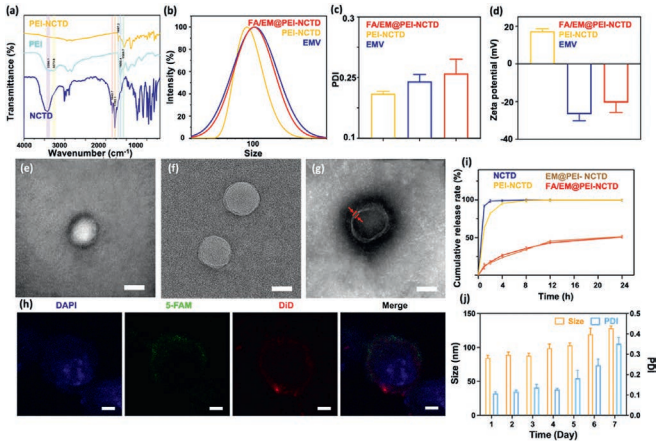


Fig. 1. *In vitro* characterization of PEI-NCTD and FA/EM@PEI-NCTD. (a) Fourier transform infrared (FTIR) analysis of PEI-NCTD. Hydrodynamic size (b), PDI (c), and zeta potential studies (d) of PEI-NCTD and FA/EM@PEI-NCTD by dynamic light scattering (DLS) ($n = 3$). The transmission electron microscopic (TEM) images (scale bar: 50 nm) of (e) PEI-NCTD, (f) empty erythrocyte membrane vesicles (EMVs), and (g) FA/EM@PEI-NCTD. (h) Fluorescence co-localization analysis based on confocal laser scanning microscopy (CLSM) (scale bar: 2 μm) identified by 5-FAM-labeled EM@PEI-5-FAM (green fluorescence), DiD-labeled EM and DAPI-labeled nucleus (blue fluorescence). (i) *In vitro* drug release profile ($n = 3$). (j) Stability study of FA/EM@PEI-NCTD in terms of particle size and PDI in phosphate buffer saline (PBS) (pH 7.4) for 7 days ($n = 3$). Data are presented as mean ± standard deviation (SD).

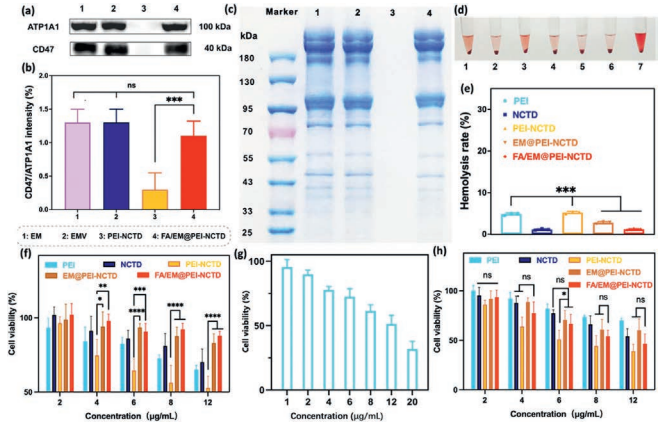


Fig. 2. Protein expression, *in vitro* biocompatibility and efficacy. (a) WB analysis and (b) quantitative assessment of ATP1A and CD47 protein expression on (1) EM, (2) EMVs, (3) PEI-NCTD, (4) FA/@PEI-NCTD ($n = 3$). (c) Total protein analysis of (1) EM, (2) EMVs, (3) PEI-NCTD, (4) FA/@PEI-NCTD *via* SDS-PAGE. Hemolysis assay: (d) Representative images (lanes 1–7 correspond to PEI, NCTD, PEI-NCTD, EM@PEI-NCTD, FA/EM@PEI-NCTD, 0.9 % NaCl, and H_2O); (e) hemolysis rate analysis ($n = 3$). (f) Viability of HEK-293 cells treated with different drug formulations ($n = 5$). (g) Viability of H22 cells treated with NCTD ($n = 5$). (h) Viability of H22 cells treated with different drug formulations ($n = 5$). Data are presented as mean ± SD. ns, non-significant. $^{***}P < 0.001$.

respectively, reflecting a clear charge reversal due to the erythrocyte membrane coating (Fig. 1d). Since NCTD lacks intrinsic fluorescence and cannot be easily labeled, we employed 5-carboxyl fluorescein (5-FAM, green fluorescence) instead of NCTD to prepare PEI-5-FAM. EM was labeled with DiD (red fluorescence), and nuclei were stained with 4′,6-diamidino-2-phenylindole (DAPI). Fluorescence distribution was visualized using CLSM. Fig. 1h shows that the green and red fluorescence signals were co-localized and distributed around the periphery of the cell nucleus, verifying the successful coating of PEI-5-FAM with EM.

The release behavior of PEI-NCTD, EM@PEI-NCTD and FA/EM@PEI-NCTD were studied to evaluate the sustained-release performance of the delivery systems. From Fig. 1i, EM@PEI-NCTD and FA/EM@PEI-NCTD exhibited significantly slower release rates than NCTD and PEI-NCTD. This can be attributed to the small molecular weight of free NCTD [24], which enabled it to rapidly permeate through the dialysis membrane, resulting in a cumulative release rate of 91.91 % ± 1.18 % within 1 h. Conversely, the cumulative release rates of EM@PEI-NCTD and FA/EM@PEI-NCTD over 24 h was 51.47 % ± 1.97 % and 50.82 % ± 1.03 %, respectively, confirming the sustained-release effect of our drug delivery system.

The stability of PEI-NCTD, EM@PEI-NCTD and FA/EM@PEI-NCTD were also assessed. Fig. 1j shows the particle size and PDI of EM@PEI-NCTD and FA/EM@PEI-NCTD remained stable in 7 days. In contrast, PEI-NCTD exhibited a gradual increase in both particle size and PDI starting from day 3, suggesting aggregation over time. The result demonstrates that EM modification enhances the dispersion stability of nanoparticles, likely by providing a protective biomimetic interface [25–27].

To confirm that membrane protein composition, particularly CD47 expression, remained intact during nanoparticle fabrication, we performed sodium dodecyl sulfate-polyacrylamide gel electrophoresis (SDS-PAGE) and Western blot (WB) analyses. As shown in Figs. 2a–c, no significant changes were observed in either the overall protein profile or CD47 expression levels.

Subsequently, we evaluated the *in vitro* function of FA/EM@PEI-NCTD. Hemolysis assays (Figs. 2d and e) revealed that the hemolysis rates of PEI, NCTD, PEI-NCTD, EM@PEI-NCTD and FA/EM@PEI-NCTD were 4.31 % ± 0.22 %, 0.93 % ± 0.12 %, 4.56 % ± 0.38 %, 2.38 % ± 0.18 % and 1.27 % ± 0.25 %, respectively, suggesting that the encapsulation strategy notably reduced the hemolytic potential of PEI-NCTD, with FA/EM@PEI-NCTD demonstrating superior blood compatibility.

The cytotoxicity of FA/EM@PEI-NCTD on normal human embryonic kidney cells (HEK-293) was investigated using the CCK-8 assay. As illustrated in Fig. 2f, PEI-NCTD exhibited the highest cytotoxicity among all groups. In contrast, FA/EM@PEI-NCTD maintained relatively high cell viability across various concentrations, indicating favorable biocompatibility.

Moreover, the anticancer efficacy was evaluated using mice hepatoma cells (H22). When NCTD was incubated with H22 cells at a concentration of 1 μg/mL, the cell viability remained at 95.50 % ± 5.85 %, indicating negligible inhibitory effects. However, at an elevated concentration of 20 μg/mL, H22 cell viability sharply decreased to 32.00 % ± 5.82 % (Fig. 2g). Fig. 2h shows that PEI-NCTD and FA/EM@PEI-NCTD demonstrated significantly enhanced cytotoxic effects compared to free NCTD at equivalent concentrations. A concentration-dependent increase in cytotoxicity was also observed. These results indicate that conjugation with PEI enhances the antitumor activity of NCTD, and the FA/EM@PEI-NCTD system effectively combines therapeutic potency with improved biosafety.

Cellular uptake of FA/EM@PEI-NCTD by H22 cells was investigated using CLSM and flow cytometry. As shown in Fig. 3a, nanoparticles labeled with 5-FAM exhibited punctate green fluorescence localized around the nucleus, indicating successful internalization. To examine the uptake further quantitatively by H22 cells, the fluorescence intensity was measured *via* flow cytometry. According to Fig. 3b, the curves of PEI-5-FAM, EM@PEI-5-FAM, and FA/EM@PEI-5-FAM significantly shifted to the right compared to the control group, confirming that H22 cells had taken up the nanoparticles, which was consistent with the CLSM results. Quantitative analysis of mean fluorescence intensity (MFI) (Fig. 3c) revealed that PEI-5-FAM achieved markedly higher uptake efficiency, likely due to the cationic nature of PEI enhancing cellular internalization. Furthermore, FA/EM@PEI-5-FAM exhibited significantly greater MFI than EM@PEI-5-FAM, indicating that FA modification enhanced tumor-targeting efficiency *in vitro*. We further examined nanoparticle uptake in RAW 264.7 cells. As presented in Figs. 3d–f,

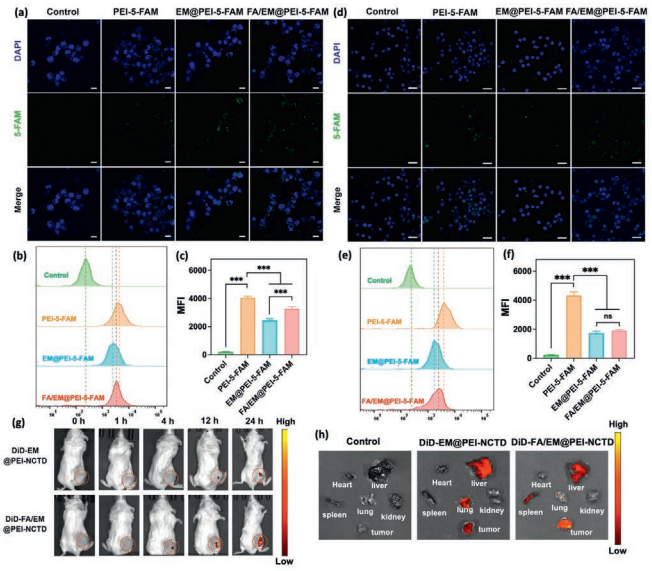


Fig. 3. Analysis of targeting and internalization behavior *in vitro*. (a) *In vitro* uptake analysis of free 5-FAM and 5-FAM-labeled nanomedicine in H22 cells was performed by CLSM (scale bar: 10 μm). Analysis of H22 cells uptake: (b) Flow cytometry histogram and (c) mean fluorescence intensity quantification ($n = 3$). (d) CLSM images of RAW 264.7 cells uptake (scale bar: 20 μm). Analysis of RAW 264.7 cells uptake: (e) Flow cytometry histogram and (f) mean fluorescence intensity quantification ($n = 3$). (g) Fluorescence signal distribution in mice over time (tumor regions highlighted with red dashed circles). (h) Analysis of fluorescence intensity in organs and tumors of mice at 24 h post-injection. Data are presented as mean ± SD. $^{***}P < 0.001$.

PEI-5-FAM displayed the highest MFI among all groups. However, the presence of EM significantly reduced the uptake of EM@PEI-NCTD and FA/EM@PEI-NCTD. Importantly, no significant difference was observed between the MFI of these two EM-coated groups, confirming that FA modification did not impair the CD47-mediated reduction in macrophage uptake [20,28,29].

To further verify the *in vivo* targeting capability of the nanoplatform, fluorescence imaging was conducted (Figs. 3g and h). The fluorescence signals in tumor tissues of the DiD-FA/EM@PEI-NCTD group were stronger than that of the DiD-EM@PEI-NCTD group, confirming that FA modification notably increased tumor accumulation efficiency *in vivo* [30]. Additionally, a strong fluorescence signal was also observed in the liver, indicating a preferential hepatic distribution, which is expected for targeted HCC therapy. All the experiments involving animals were conducted in accordance with the guidelines for the care and use of laboratory animals of Shanghai Jiao Tong University and were approved by the Animal Ethics Committee (approval No. 202501407).

For *in vivo* antitumor evaluation, a subcutaneous HCC mouse model was established. Five mice from the same cohort were randomly designated as the Normal group and were not subjected to H22 tumor cell inoculation, while the remaining mice received subcutaneous tumor implantation. Once tumors reached 80–100 mm^3, mice were randomized into six groups ($n = 5$ per group). The treatment strategy is illustrated in Fig. 4a. Survival analysis (Fig. S1 in Supporting information) showed that the median survival of mice treated with FA/EM@PEI-NCTD was significantly extended to 49 days, compared to 21 days in the control group and 31 days in the free NCTD group. Fig. S2e (Supporting information) indicates that NCTD and its delivery systems elevated white blood cell counts, consistent with previous findings [31].

Notably, mice in the FA/EM@PEI-NCTD group exhibited hematological parameters similar to those of the normal group, whereas PEI-NCTD treatment led to decreased red blood cell counts, hemoglobin levels, and platelet counts, suggesting potential hemolytic toxicity.

As shown in Figs. S2–S4 (Supporting information), the levels of alanine aminotransferase (ALT) and aspartate aminotransferase (AST) in the control group and PEI group were higher, indicating hepatic injury (Figs. S2a–d). In the NCTD group, a significant reduction in blood urea nitrogen (BUN) and an increase in creatinine (CREA) levels were observed, reflecting nephrotoxic effects. In contrast, the FA/EM@PEI-NCTD group exhibited no kidney damage. Fig. S3a revealed that the weights of mice in PEI-NCTD group were significantly lower than the Control group, indicating the toxicity of PEI-NCTD, while the mice receiving FA/EM@PEI-NCTD maintained stable body weight increases throughout treatment. Moreover, organ index analysis (Fig. S3b) showed no notable differences in organ weights between the FA/EM@PEI-NCTD and Normal groups. From Fig. S4, the renal tissues of mice treated with NCTD exhibited signs of renal interstitial edema and necrosis of tubular epithelial cells (highlighted by black arrows), confirming renal toxicity. However, kidneys from the FA/EM@PEI-NCTD group appeared histologically normal, further verifying the biocompatibility of the NCTD drug delivery system.

As illustrated in Figs. 4b and c, mice treated with FA/EM@PEI-NCTD demonstrated the slowest tumor growth rate, as evidenced by the minimal increase in tumor volume over time. Correspondingly, Fig. 4d shows that the average tumor weight in the control group was 0.82 ± 0.14 g, significantly higher than that in the EM@PEI-NCTD and FA/EM@PEI-NCTD groups, which were 0.45 ± 0.08 g and 0.40 ± 0.10 g, respectively. Tumor inhibition rates (TIR) further confirmed the therapeutic advantage of FA/EM@PEINCTD (Fig. 4e). Specifically, the TIRs for the PEI, NCTD, PEI-NCTD, EM@PEI-NCTD, and FA/EM@PEI-NCTD groups were $4.4\% \pm 3.4\%$, $28.0\% \pm 5.1\%$, $40.0\% \pm 8.5\%$, $42.6\% \pm 3.6\%$, and $49.0\% \pm 6.4\%$, respectively. Compared with free NCTD group, the FA/EM@PEI-NCTD group exhibited a significantly higher inhibition rate, highlighting its enhanced antitumor efficacy *in vivo*. From the H&E staining of Fig. 4f, tumor cells in all groups showed abnormal morphology like disordered arrangement, enlarged nuclei with hyperchromasia, and pleomorphic features including megakaryocytes, binucleation, and multinucleation. In contrast to the Control and PEI groups, which displayed no significant pathological alterations, tumor tissues from the NCTD, PEI-NCTD, EM@PEI-NCTD, and FA/EM@PEI-NCTD groups demonstrated pronounced nuclear condensation, fragmentation, and dissolution (indicated by black arrows), suggesting killing effect on tumor cells. Quantitative analysis of TUNEL staining (Fig. 4g) demonstrated fluorescence intensity positively correlated with apoptosis rate. EM@PEI-NCTD ($14.62\% \pm 0.99\%$) and FA/EM@PEI-NCTD ($16.39\% \pm 0.51\%$) exhibited peak apoptosis rates, significantly exceeding NCTD and PEI-NCTD groups ($P < 0.001$), validating enhanced tumor cytotoxicity through the delivery system. Additionally, ImageJ quantification of Ki-67 staining (Fig. 4h) showed highest Ki-67 positivity in these groups ($37.56\% \pm 2.67\%$ and $34.42\% \pm 0.72\%$, respectively; $P < 0.001$ *vs.* others), confirming maximal proliferation. Conversely, NCTD treatments suppressed proliferation, with FA/EM@PEI-NCTD exerting stronger inhibitory effects than NCTD, PEI-NCTD, and EM@PEI-NCTD.

As shown in Figs. S5 and S6 (Supporting information), the underlying antitumor mechanism was investigated (Fig. S5a). The results revealed that FA/EM@PEI-NCTD upregulated the expression of pro-apoptotic proteins (caspase-3 and Bax), while concurrently downregulating the anti-apoptotic protein (Bcl-2) (Figs. S5b–e), suggesting that the therapeutic effect of FA/EM@PEI-NCTD was mediated by the induction of apoptosis and suppression of tumor cell proliferation. Quantitative analyses confirm that the tumor cells of FA/EM@PEI-NCTD had the highest apoptosis rate (Fig. S6).

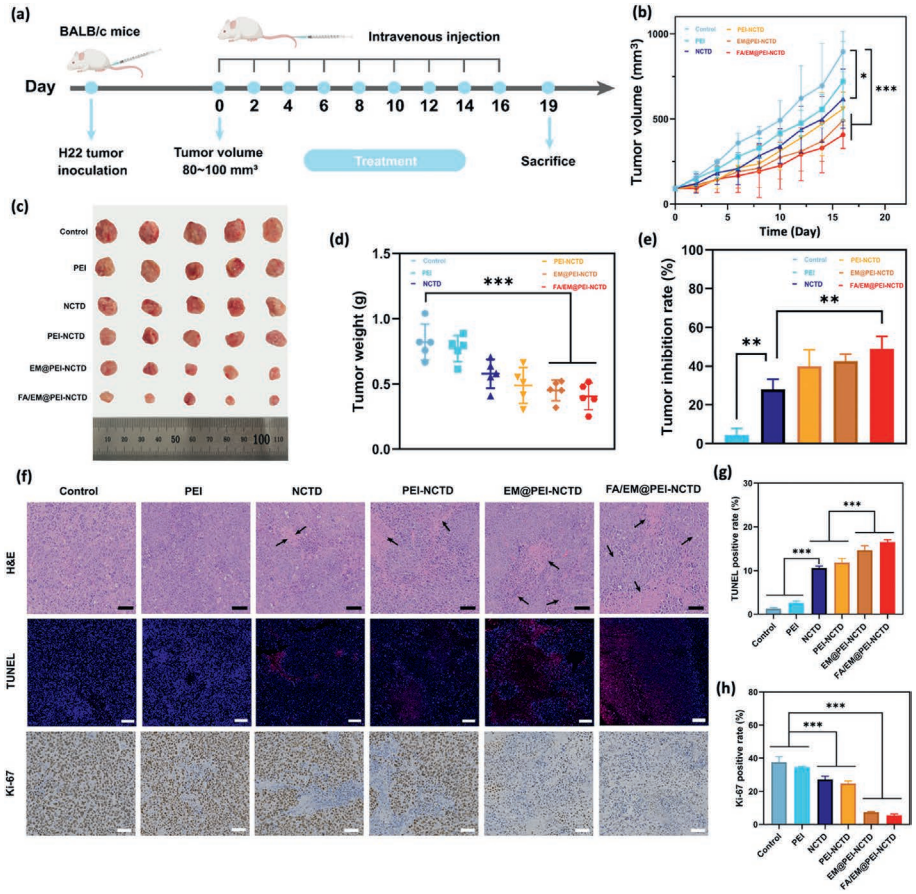


Fig. 4. *In vivo* anti-tumor efficacy. (a) Schematic diagram of tumor inoculation and treatment plan in H22 tumor model. (b) Average tumor volume change curve in different groups ($n=5$) after treatment. (c) Tumor photographs in different groups ($n=5$) at the end of treatment. (d) Tumor weight comparison in mice ($n=5$) after treatment. (e) Tumor inhibition rate analysis in different groups ($n=5$) at the end of treatment. (f) Histological analysis of mouse tumor tissue using hematoxylin and eosin (H&E) staining (scale bar: 50 μm), black arrows highlight regions exhibiting injury; CLSM images of TdT-mediated dUTP nick-end labeling (TUNEL) staining (scale bar: 100 μm) of mice tumors and microscopy images of Ki-67 staining (scale bar: 50 μm) of mice tumors. (g) Quantitative analysis of fluorescence positivity of TUNEL staining of mice tumors ($n=5$). (h) Quantitative analysis of immunohistochemical positivity of Ki-67 staining of mice tumors ($n=5$). Data are presented as mean ± SD. $^{*}P<0.05$, $^{**}P<0.01$, $^{***}P<0.001$.

This study developed a novel targeted drug delivery system for hepatocellular carcinoma, FA/EM@PEI-NCTD. The system was constructed by synthesizing PEI-NCTD nanoparticles *via* ionic interaction, coating them with erythrocyte membranes, and conjugating folic acid ligands. PEI-NCTD provided high drug loading, EM coating reduced macrophage uptake, and FA modification enhanced tumor cell targeting. *In vivo*, the system prolonged survival, inhibited tumor growth, and reduced NCTD-induced nephrotoxicity in H22 tumor-bearing mice, while maintaining normal hematological, biochemical, and histological parameters. Fluorescence imaging confirmed enhanced tumor accumulation, and mechanistic studies showed promotion of apoptosis (upregulated caspase-3, Bax; downregulated Bcl-2). Overall, FA/EM@PEI-NCTD offers an effective strategy to improve NCTD's therapeutic potential in liver cancer.

CRediT authorship contribution statement

Hang Xiao: Writing – review & editing, Writing – original draft, Visualization, Validation, Methodology, Formal analysis, Data curation. **Hongyu Zhong:** Writing – review & editing, Visualization, Software, Formal analysis, Data curation, Conceptualization. **Shiqi Yang:** Visualization, Validation, Software, Resources, Investigation, Formal analysis, Data curation. **Kunwei Li:** Validation, Methodology, Investigation, Formal analysis, Data curation, Conceptualization. **Jing Su:** Visualization, Validation, Methodology, Investigation, Formal analysis, Data curation, Conceptualization. **Faisal Raza:** Writing – review & editing, Writing – original draft, Supervision, Software, Resources, Project administration, Investigation. **Mingfeng Qiu:** Supervision, Software, Resources, Project administration, Methodology, Investigation, Formal analysis, Data curation, Conceptualization.

Declaration of competing interest

The authors declare that they have no known competing financial interests or personal relationships that could have appeared to influence the work reported in this paper.

Acknowledgments

This work was supported by the National Natural Science Foundation of China (Nos. 82374149, 81973487), Yunnan Provincial Department of Science and Technology Project of "Yunnan Qiu Mingfeng Expert Workstation" (No. 202305AF150141), National Science and Technology Major Projects for "Major New Drugs Innovation and Development" (No. 2018ZX09711003–008–002) and China Postdoctoral Science Foundation (No. 2025M773886).

Supplementary materials

Supplementary material associated with this article can be found, in the online version, at doi:10.1016/j.cclet.2025.111937.

References

[1] Q. Wang, Y. Sun, L. Lai, et al., Chin. Chem. Lett. 36 (2025) 110212.
[2] F. Bray, M. Laversanne, H. Sung, et al., CA Cancer J. Clin. 74 (2024) 229–263.
[3] J.M. Llovet, R. Pinyol, M. Yarchoan, et al., Nat. Rev. Clin. Oncol. 21 (2024) 294–311.
[4] A.G. Singal, J.M. Llovet, M. Yarchoan, et al., Hepatology 78 (2023) 1922–1965.
[5] B. Zeng, X. Chen, L. Zhang, et al., Medicine 103 (2024) e37394.
[6] Z. Ding, B. Xu, H. Zhang, et al., Molecules 28 (2023) 7609.
[7] M.S. Pan, J. Cao, Y.Z. Fan, Chin. Med. 15 (2020) 55.
[8] L. Mei, W. Sang, K. Cui, et al., Cancer Sci. 110 (2019) 582–595.
[9] B. Gao, J. Luo, Y. Liu, et al., Int. J. Nanomed. 16 (2021) 4073–4085.
[10] G. Martínez-Razo, P.C. Pires, A. Avilez-Colin, Int. J. Mol. Sci. 26 (2025) 1215.
[11] X. Zhang, Z. He, Int. J. Nanomed. 18 (2023) 7729–7744.
[12] J.Y. Chiang, T.H. Lin, J.X. Cheng, W.Y. Pan, Int. J. Biol. Macromol. 306 (2025) 141336.
[13] F. Meng, J. Wang, Y. He, et al., Proc. Natl. Acad. Sci. U. S. A. 119 (2022) e2122595119.
[14] Y. Wang, C. Zhang, S. Han, et al., Chin. Chem. Lett. 35 (2024) 109578.
[15] H. Zhang, B. Wang, J. Han, et al., Chin. Chem. Lett. 36 (2025) 110319.
[16] C.F. Rodrigues, I.J. Correia, A.F. Moreira, Int. J. Pharm. 655 (2024) 124007.
[17] M. Li, H. Fang, Q. Liu, et al., Biomater. Sci. 8 (2020) 1802–1814.
[18] X. Wang, K. Mao, X. Zhang, et al., Interdiscip. Med. 2 (2024) e20240014.
[19] F. Yuan, C. Zhang, X. Luo, et al., Chem. Sci. 14 (2023) 14182–14192.
[20] F. Raza, L. Jiang, S. Zhang, et al., Chem. Eng. J. 491 (2024) 151709.
[21] Y. Zhong, Z. Qiu, Y. Li, et al., Chin. Chem. Lett. 36 (2025) 109846.
[22] J. Du, S. Zhou, Y. Ma, et al., Colloids Surf. B: Biointerfaces 234 (2024) 113721.
[23] L. Zhou, Y. Du, Y. Shang, et al., Int. J. Nanomed. 19 (2024) 12975–12998.
[24] Y. Li, Y. Xiao, H.P. Lin, et al., Biomaterials 188 (2019) 160–172.
[25] J. Liao, L. Gong, Q. Xu, et al., Adv. Mater. 36 (2024) e2402445.
[26] N. Kostevsek, Biomater. Adv. 170 (2025) 214234.
[27] Y. Gao, R. Zhou, Q. Wang, et al., Chin. Chem. Lett. 35 (2024) 109521.
[28] X. Wang, H. Li, X. Liu, et al., Biomaterials 143 (2017) 130–141.
[29] C.M. Hu, R.H. Fang, B.T. Luk, et al., Nanoscale 5 (2013) 2664–2668.
[30] R. Chang, X. Qu, Y. Ye, et al., Chin. Chem. Lett. 36 (2025) 110802.
[31] L. Liang, L. Zhao, Y. Wang, et al., Mol. Pharm. 18 (2021) 1003–1013.